Science of the Total Environment 917 (2024) 170478

Contents lists available at ScienceDirect

Science of the Total Environment

journal homepage: www.elsevier.com/locate/scitotenv

# Elucidating phosphorus removal dynamics in a denitrifying woodchip bioreactor

Gimhani N. Perera [a,b], Dorisel Torres Rojas [a], Aldrin Rivas [c], Greg Barkle [d], Brian Moorhead [c], Louis A. Schipper [a], Rupert Craggs [b], Adam Hartland [a,c,*]

[a] Environmental Research Institute, School of Science, Faculty of Science and Engineering, University of Waikato, Kirikirioa Hamilton, New Zealand
[b] National Institute of Water and Atmospheric Research Ltd (NIWA), PO Box 11115, Kirikirioa Hamilton 3251, New Zealand
[c] Lincoln Agritech Ltd, Ruakura, Kirikirioa Hamilton 3214, New Zealand
[d] Land and Water Research Ltd, Kirikirioa Hamilton 3217, New Zealand

## HIGHLIGHTS

- Denitrifying bioreactors receive phosphorus from allochthonous and autochthonous sources.
- Autochthonous phosphorus is generated by reduction of iron (hydr)oxides within reactors.
- Coupled iron-phosphorus cycles explain phosphorus source vs sink behaviour.
- Phosphorus removal rates can be of similar magnitude to nitrate removal rates.

## GRAPHICAL ABSTRACT

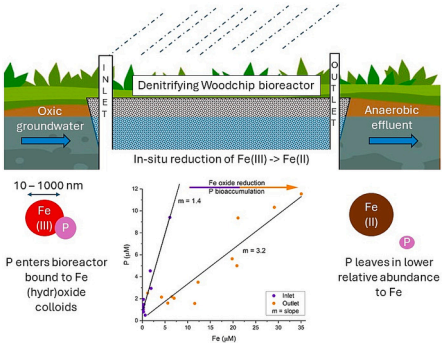


## ARTICLE INFO

Editor: Yifeng Zhang

*Keywords:*
Phosphorus
Denitrifying woodchip bioreactor
Biological uptake
Biogeochemical cycles

## ABSTRACT

Denitrifying woodchip bioreactors (DBRs) are an established nitrate mitigation technology, but uncertainty remains on their viability for phosphorus (P) removal due to inconsistent source-sink behaviour in field trials. We investigated whether iron (Fe) redox cycling could be the missing link needed to explain P dynamics in these systems. A pilot-scale DBR (Aotearoa New Zealand) was monitored for the first two drainage seasons (2017–2018), with supplemental in−field measurements of reduced solutes ($Fe^{2+}$, $HS^-/H_2S$) and their conjugate oxidised species ($Fe^{3+}/SO_4^{2-}$) made in 2021 to constrain within-reactor redox gradients. Consistent with thermodynamics, the dissolution of $Fe^{3+}_{(s)}$ to $Fe^{2+}_{(aq)}$ within the DBR sequentially followed $O_2$, $NO_3^-$ and $MnO_{2(s)}$ reduction, but occurred before $SO_4^{2-}$ reduction. Monitoring of inlet and outlet chemistry revealed tight coupling between Fe and P (inlet $R^2$ 0.94, outlet $R^2$ 0.85), but distinct dynamics between drainage seasons. In season one, outlet P exceeded inlet P (net P source), and coincided with elevated outlet $Fe^{2+}$, but at ~50 % lower P concentrations relative to inlet Fe:P ratios. In season 2 the reactor became a net P sink, coinciding with declining outlet $Fe^{2+}$ concentrations (indicating exhaustion of $Fe^{3+}_{(s)}$ hydroxides and associated P). In order to characterize P removal under varying source dynamics (i.e. inflows vs *in-situ* P releases), we used the inlet Fe vs P relationship to

* Corresponding author. at: Environmental Research Institute, School of Science, Faculty of Science and Engineering, University of Waikato, Kirikirioa Hamilton, New Zealand.
*E-mail address:* adam.hartland@waikato.ac.nz (A. Hartland).

https://doi.org/10.1016/j.scitotenv.2024.170478
Received 3 October 2023; Received in revised form 23 January 2024; Accepted 24 January 2024
Available online 30 January 2024

estimate P binding to colloidal Fe (hydr)oxide surfaces under oxic conditions, and the outlet $Fe^{2+}$ concentration to estimate *in-situ* P releases associated with Fe (hydr)oxide reduction. Inferred P-removal rates were highest early in season 1 ($k = 0.60$ g P $m^3$ $d^{-1}$; 75–100 % removal), declining significantly thereafter ($k = 0.01 \pm 0.02$ g P $m^3$ $d^{-1}$; ca. 3–67 % removal). These calculations suggest that microbiological P removal in DBRs can occur at comparable magnitudes to nitrate removal by denitrification, depending mainly on P availability and hydraulic retention efficiency.

## 1. Introduction

Denitrifying bioreactors (DBRs) are a widely employed edge−of−-field technology for the interception and removal of agricultural nitrate pollution (Blowes et al., 1994; Dougherty et al., 2020; Lepine et al., 2018). Phosphorus (P) also contributes significantly to nutrient loading in drainage, leading to eutrophication; but most DBR studies have focussed on nitrate (Schipper et al., 2010; Corbett et al., 2020), leaving an important gap in our understanding (Wu et al., 2023).

Woodchip bioreactors are known to leach P during initial commissioning (David et al., 2016). Subsequently, exhibiting consistent P removal in the order of 0.01 and 0.08 g P $m^{-3}$ $d^{-1}$ (Dougherty, 2018). While P removal has been documented in a few studies (Dougherty, 2018), there is conjecture regarding whether P removal in DBRs solely reflects biological accumulation, or whether other biogeochemical processes (e.g. adsorption, redox cycling) are involved (Sharrer et al., 2016; Sanchez Bustamante-Bailon et al., 2022; Wu et al., 2023).

To a first approximation, inconsistent P behaviour in DBRs occurs due to temporal variations in flow rates and the hydrochemistry of drainage waters, resulting from episodic flow dynamics and variable soil source chemistry. However, within-reactor biogeochemical and microbial processes are also likely to be relevant to P dynamics (Hartland et al., 2015). It is established that direct P bioaccumulation by microbes can occur in excess to requirements because bacteria utilize P and store it as intracellular polyphosphate (poly−P) (Oehmen et al., 2010). Indeed, faster P accumulation occurs under anaerobic conditions, which may favour P removal in DBRs compared to aerobic systems (Kerrn-Jespersen and Henze, 1993; Sun et al., 2020; Zaman et al., 2021), but these processes are understudied in woodchip DBRs and remain to be fully elucidated.

Biological P accumulation in DBRs may also be favoured because iron (hydr)oxides, the dominant P binding phase in aquatic systems, are unstable in anaerobic conditions (Sposito, 2004). Iron (hydr)oxides are ubiquitous in freshwater, soil, and sediment, and strongly bind orthophosphate ($PO_4^{3-}$) due to their large specific surface area and positive net surface charge at pH values <7 (Damasceno et al., 2023; Shahid et al., 2019). Hence, Fe (hydr)oxides are inevitably important vectors for P transfer into DBRs in agricultural settings; and Fe redox cycling is likely to affect P dynamics, because insoluble iron(III) (hydr)oxides undergo reductive dissolution under anaerobic conditions, simultaneously releasing P and soluble $Fe^{2+}$ ions (Hartland et al., 2015).

In this paper, we investigated the biogeochemistry of a pilot-scale DBR (Tatuanui, Waikato, Aotearoa New Zealand) including all major element redox processes, with the goal of elucidating the reaction pathways controlling phosphorus. This work also contributes to ongoing research into the attenuation of P (and potentially other pollutants) in agricultural drainage through incorporation of novel substrates in woodchip DBRs.

## 2. Materials and methods

### 2.1. Water sampling

A pilot−scale denitrifying woodchip bioreactor located in Tatuanui of the Waikato region (Rivas et al., 2020a, 2020b), Aotearoa (New Zealand), was selected for this study. The primary substrate being pine woodchips, contained within a 58 $m^3$ bioreactor of trapezoidal shape (25 $m^3$ of saturated volume), with a basal area of 5 × 9 m, a surface area of 8.4 × 12.4 m, and depth of 1.2 m. The bioreactor was installed in 2017 and monitored throughout the 2017 and 2018 drainage seasons by researchers at Lincoln Agritech Ltd. Additional sampling and monitoring was conducted during the 2021 (July–October) drainage season, to better constrain the in−situ bioreactor redox conditions. Water samples were collected every two weeks during the first two drainage seasons, and on three occasions during the 2021 drainage season. Automatic monitoring devices and sensors were attached to the inlet and outlet wells to monitor the flow rate, $NO_3^-$ concentration, temperature, and Electrical Conductivity (EC). An outlet weir recorded the flow through the bioreactor. Additional water quality measurements were made on manual (grab) samples following standard laboratory procedures (Rivas et al., 2020a, 2020b). Samples for laboratory analysis of bulk chemistry were collected in triplicate from the inlet, internal (mid) wells along the centre line of the bioreactor ($C_1$, $C_2$, $C_3$), and outlet, and filtered in-field using 0.45 μm syringe filters into 50 mL and 15 mL falcon tubes. The distances from the inlet well to the centre wells (C1, C2, C3), were approximately 2.15 m, 4.30 m, and 6.65 m, respectively; and the distance from the inlet well to the outlet well was approximately 8.65 m. These samples were collected using a flexible hose and syringe connected to a three−way valve to minimise exposure to oxygen. Samples were carefully handled to measure the concentration of reduced solutes in−field to constrain the $Fe^{2+}/Fe^{3+}$ and $HS^-/SO_4^{2-}$ redox couples. Samples for metal analysis were preserved using 2 % (*v*/v) double-distilled concentrated $HNO_3$ (Savillex DST − 1000 Acid Purification System; Eden Prairie, MN, USA) and were then stored on ice at ≤4 °C during transport.

### 2.2. Analytical chemistry

In−situ measurements of pH, temperature, DO (Dissolved Oxygen), ORP (Oxidation−Reduction Potential), Conductivity (EC), and TDS (Total Dissolved Solids) were made using a YSI ProODO probe (YSI incorporated, USA). Ferrous iron ($Fe^{2+}$) and hydrogen sulfide ($HS^{2-}$) concentrations were respectively determined by the ferrozine (Viollier et al., 2000) and methylene blue methods (Reese et al., 2011), using a portable UV−Vis spectrophotometer (HACH DR1900, USA). Offsite chemical analysis of water samples was performed at Waikato University. Total organic carbon (TOC) was measured on an OI Analytical Aurora 1030 W TOC analyser (Washington, USA), while nitrate ($NO_3^-$), sulphate ($SO_4^{2-}$), chloride ($Cl^-$), and fluoride ($F^-$) were analysed using an ICS−2000 Ion Chromatograph (Thermo Fisher, USA) using an isocratic method (5 mM KOH, 40 mins). Dissolved metals (Fe, and Mn) were determined by inductively coupled plasma mass spectrometry using an Agilent 8900 ICP − MS (Santa Clara, CA, United States), controlled by MassHunter Workstation Version 4.5 and connected to an SPS4 autosampler (Mohammadi et al., 2022). Phosphorus (ascorbic acid method) and ammonium ($NH_4^+$) concentrations were measured by UV spectrophotometry (Dynamica HALO VIS−20, UK). Finally, alkalinity was measured by using a universal digital titrator (HACH, USA) by titrating against pH with 0.15 N $H_2SO_4$ to the $CO_2$ equivalence point (pH 3.9). All the samples collected in 2021 were measured in triplicate and reported as the average and standard deviation. The statistical methods employed were Pearson's correlation analysis (Microsoft Excel Version 2311), and least squares regression (Grapher v22).

### 2.3. Hydrogeochemical simulations

The dataset for the year 2021 was simulated to determine the saturation indices of $Fe(OH)_3$ and FeS. However, the simulations could not be conducted for the data in 2017 and 2018 because the redox species ($Fe^{2+}$ and $HS^-$) were not measured during routine monitoring. Prior to the hydro chemical simulations, input data were screened for gross errors using the charge balance error (CBE) metric, after which solutions were adjusted to charge neutrality within PHREEQC 3.0 (Parkhurst, 1995) by adding $Cl^-$ and $Na^+$, since neither ion strongly affects the studied equilibria. Generally, the percent charge−balance error before adjustment was <5 %, reflecting a representative and accurate analysis of the studied solutions. PHREEQC scripts and the raw data used in these simulations are provided in the Supplementary Information (**Table S1**). Equilibrium speciation calculations based on the aforementioned monitoring data were also performed in PHREEQC 3.0, with particular attention paid to the accurate representation of the redox equilibrium along the reactors' length, to accurately determine the solubility of amorphous iron (hydr)oxides and the potential for formation of other reaction by-products (i.e., iron sulfide precipitates). Outputs from these simulations included the speciation of major and minor ions, saturation indices of amorphous $Fe(OH)_3$ and FeS precipitates, and could be extended in the future to include the interaction of the aqueous species with iron hydroxide surfaces (Charlton and Parkhurst, 2011; Dzombak and Morel, 1991). Hence, the general modelling framework employed here, allows for the calculation of saturation indices (a measure of mineral solubility) as constrained by in-field measurements of redox couples, and the distribution of aqueous species along the reactors' length (respecting the gradation from oxidising to reducing conditions).

## 3. Results

### 3.1. Bioreactor trends in redox-active species

Results of bioreactor monitoring over two consecutive drainage seasons are presented in Fig. 1 (**Table S2**), which shows the net change in N, Mn, Fe, P, and S between inlet and outlet ($\Delta_x = x_{out} - x_{in}$). These elements are included in this analysis because they constitute the main inorganic electron−accepting components involved in natural biogeochemical cycles (Stumm and Morgan, 1996).

In season 1, the reactor leached Mn, Fe and P. Concentrations of Fe, Mn and P declined exponentially from initial high values in season 1 and continued to decline into season 2. Outlet concentrations of Fe and P showed close covariation throughout season 1 ($R^2 = 0.86$), but then decoupled during season 2 ($R^2 = 0.11$). Over both periods, the reactor actively removed $NO_3^-$, but only minimal changes occurred in $SO_4^{2-}$ concentrations between inlet and outlet, with the exception of higher sulfate removal under stagnant (no flow) conditions, toward the end of season 1.

Overall, the bioreactor was a nitrate and sulfate sink during both drainage seasons, but deviated from source−to−sink behaviour for P, over this period. Outlet manganese and iron concentrations were both highest following the commissioning of the bioreactor in 2017, then gradually diminished during the 2018 season. Throughout this period, iron and phosphorus remained tightly correlated (Fig. 2) at both inlet and outlet. Fe:P ratios were generally higher in inlet water compared to the outlet, where they remained correlated, but at a lower Fe:P ratio, indicating P loss (relative to Fe) along the flow path.

The hydrology of the bioreactor fluctuated significantly across the first two drainage seasons. Cumulative flows for 2017 (season 1) and 2018 (season 2) were 337 $m^3$ and 952 $m^3$, respectively; and peak flows were 28.8 $m^3$ $day^{-1}$ and 100 $m^3$ $day^{-1}$, respectively (Rivas et al., 2020a, 2020b). The drainage seasons also differed substantially in their duration, with season 2 being much shorter than season 1, but with a cumulative drainage of ca. three times that of season 1. Accordingly, flashy (event) flows account for some of the observed dynamics in nutrient

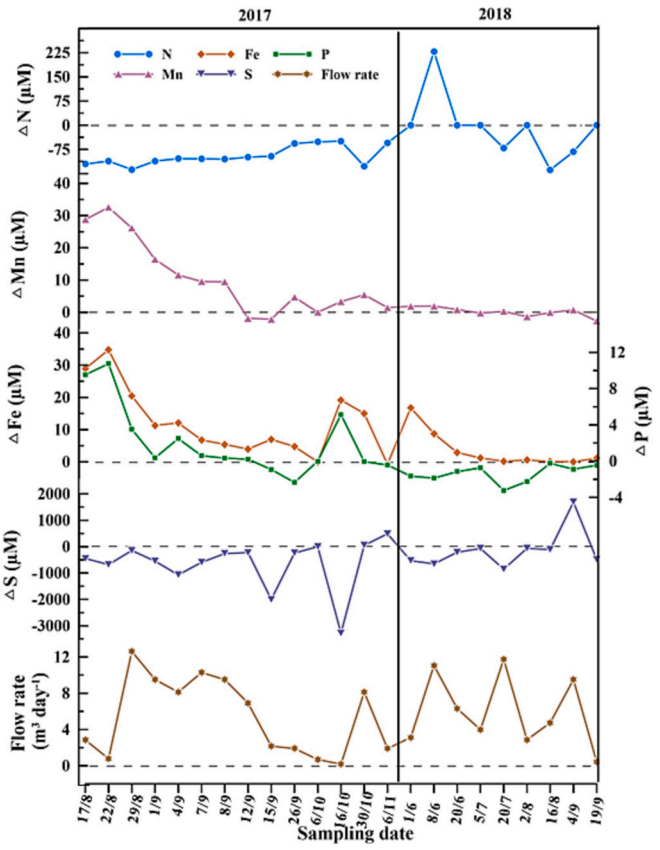


**Fig. 1.** Net change in N, Mn, Fe, S, and P (μM) (outlet−inlet) plotted with flow rate ($m^3$ $d^{-1}$) for the 2017 and 2018 drainage seasons.

removal. For example, the high outlet N concentration in season 2 corresponded to a high−flow event (0.23 mM; 11 $m^3$ $day^{-1}$), and conversely, an interval of pronounced S − removal was observed at low flows, when more reduced conditions were favoured in season 1 ($\Delta S = -3.28$ mM; 0.17 $m^3$ $day^{-1}$ (Fig. 1)).

The results of PHREEQC modelling of the 2021 field data provide a more detailed picture of the underlying hydrogeochemical processes leading to shifts in the concentration of redox−active components between inlet and outlet. Fig. 2 shows the concentrations of nitrate, manganese, iron, and sulphate along the reactors' length, alongside derived saturation index values for common Fe minerals.

The hydrogeochemical simulations suggest that the consumption of all five major oxidizers (electron acceptors) present in the bioreactor influent ($O_2$, N(V), Mn(IV), Fe(III), S(VI)) were removed to some extent along the reactors' length, with Fe(III) and Mn(IV) reduction being shown by increases in the reaction products (Fe(II) and Mn(II)) (Fig. 2) (see **Table S3** for DO values). Consequently, the derived mineral saturation indices for Fe (hydr)oxides indicate oversaturated conditions in the inlet water ($SI_{Fe(OH)3} > 0$), but undersaturated conditions by the first centre well, trending to lower $SI_{Fe(OH)3}$ values in the downstream centre wells and the outlet of the bioreactor. Iron sulfide ($SI_{FeS}$) conversely remained undersaturated, despite increases in $Fe^{2+}$ and $HS^-$ (**Table S1**) along the flow path.

### 3.2. Changes in Fe and P dynamics with bioreactor age

Fig. 3 shows the correlation between Fe and P in the 2017 and 2018 monitoring data. Inlet samples in both season 1 and season 2 were characterised by steeper relationships (m = 1.449), compared to the outlet. In season 1, the correlation between Fe and P at the outlet was characterised by a much shallower slope (m = 0.3289) and higher Fe:P

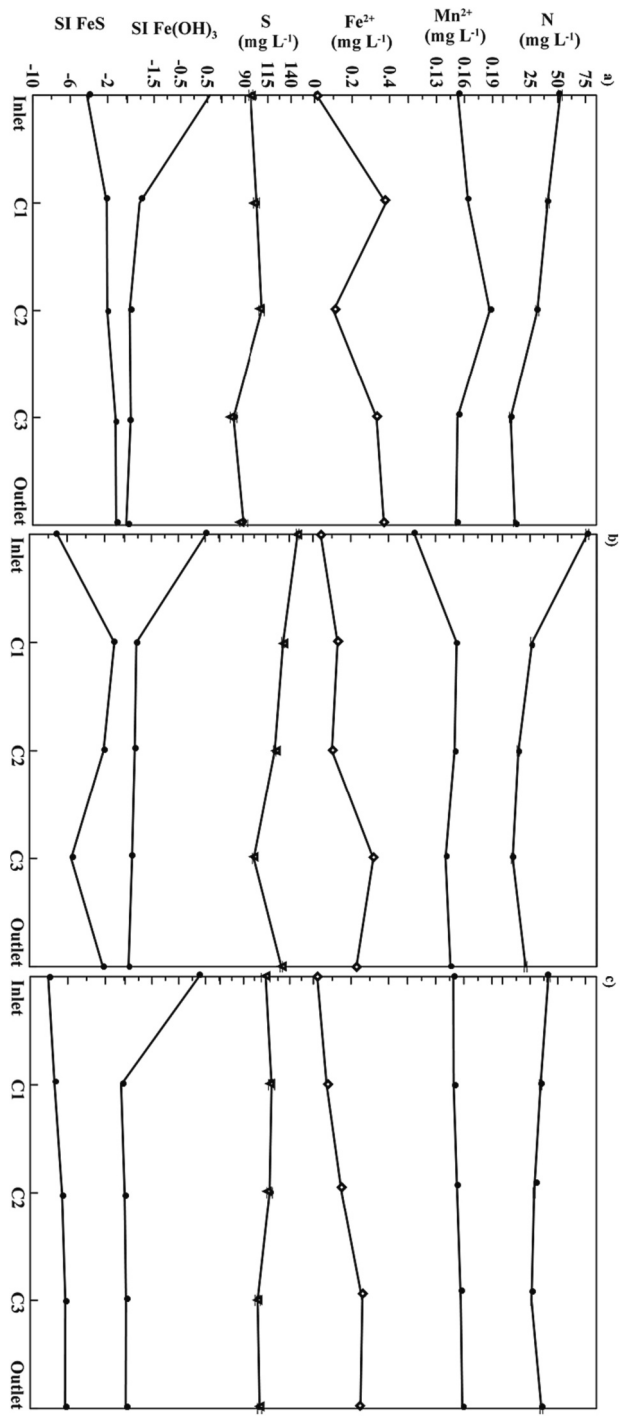


**Fig. 2.** Longitudinal trends in bioreactor hydrochemistry (data from the **2021 drainage season** 27th July, 17th Aug., 27th Sep). Results of hydrochemical simulations include saturation index (SI) values for two primary Fe minerals (amorphous iron hydroxide ($Fe(OH)_3$(a); and iron monosulfide (FeS)) and total N and S ($SO_4^{2-}$) concentrations plotted as a function of distance along the bioreactor alongside the products of Fe(III) and Mn(IV) reduction (Fe(II), Mn(II)).

ratios, consistent with P attenuation with respect to Fe within the DBR. However, in the subsequent season (2018), the outlet Fe and P were uncorrelated, indicating higher P retention within the reactor, and overall lower levels of Fe(III) reduction than observed in season 1.

## 4. Discussion

### 4.1. Redox biogeochemistry and denitrifying bioreactors

DBRs are engineered for denitrification. They provide a means to address diffuse nitrate pollution from the agricultural sector, and are most suitable where flow is channelled (i.e. by tile drainage). Once dissolved oxygen in drainage water is depleted, DBR's remove nitrate by supplying organic carbon as an energy source, thereby establishing a carbon-rich anaerobic environment for denitrifying microorganisms (Fan et al., 2022). Although recent studies have shown the potential for DBR's to remove phosphorus (Christianson et al., 2021; Povilaitis et al., 2020; Table 1), the underlying mechanisms of P removal remain to be fully described, limiting next-generation DBR designs that additionally target P removal. As shown by this study, beyond denitrification, a range of biogeochemical cycles operate in DBRs which correlate with P dynamics. In the following discussion, we explore the potential of redox transformations to explain P dynamics in DBRs. We also discuss the potential for Fe oxides to be harnessed to remediate P pollution.

### 4.2. Within−reactor trends in redox explain P dynamics

Denitrification is one of many possible reaction pathways between (oxidised) solutes and (reduced) organic carbon in DBRs (Blowes et al., 1994). A series of biogeochemical changes can be predicted based on the free−energy change of reaction ($\Delta G^{\circ}$) between reactants and products, in which oxidizers (electron acceptors) are removed sequentially, from most energetic ($O_2 > NO_3^-$), through the energetically−intermediate solids ($MnO_2$, $Fe(OH)_3$), to the least energetic and most abundant remaining oxidant ($SO_4^{2-}$) (**Fig. 3.b**). We note that terminal respiration of bicarbonate (C(IV)) to methane is generally avoided due to relatively high concentrations of sulfate (S(VI)) throughout the Tatuanui DBR, but may be more prevalent in less S-enriched settings. These reactions all proceed due to the ready supply of organic carbon, and the presence of microorganisms and dissolved/particulate electron acceptors in the water (Addy et al., 2016; Christianson et al., 2012; Thapa et al., 2023). Despite hydrologic variations, our results (**Fig. 2**) demonstrate that longitudinal changes in the Tatuanui DBR coherently followed the redox ladder (**Fig. 3.b**), after the initial rapid removal of oxygen between the inlet and first centre well (C1). In sequence, facultative bacteria then consumed nitrate, followed by manganese and iron oxides (forming Fe (II), Mn(II)), and finally sulphate, producing hydrogen sulfide, $H_2S_{(g)}$, which can commonly be smelt in DBR piezometers.

In principle, the progression of less energetic redox transformations (such as sulfate reduction; Fig. 3) within any DBR will be determined by carbon supply (assumed to be sufficient to maintain a long−term nitrate removal rate), nitrate supply, and the hydraulic residence time (HRT) of the water in the bioreactor (Schipper et al., 2010). Following oxygen and nitrate removal, the anaerobic DBR environment promotes dissimilatory manganese and iron reduction (where oxides are present), followed by the reduction of sulfate (Fig. 2). Hence, the detection of $H_2S$(g) in reactor piezometers, confirms that DBRs can naturally oscillate across a wide range of redox potentials depending on flow and nitrate supply (**Fig. 3**).

In the context of the redox ladder (Fig. 3), the observed emission of Fe(II) and Mn(II) from the outlet of the Tatuanui DBR in season 1, was therefore consistent with N-limitation and the gradual reduction of soil-derived Mn and Fe oxides likely incorporated either during reactor construction, leached from the 0.7 m topsoil above the uppermost woodchip layer (Rivas et al., 2023), or washed into the reactor during high flows (Fig. 1). Furthermore, because natural Fe (hydr)oxides adsorb and transport P (Saeed et al., 2018), but only the carrier phase (i.e. Fe (III) + e→ Fe(II)) becomes reduced, any inorganic P released via this process becomes available for other reactions, including cellular uptake. Therefore, the monitoring results presented here suggest that as the reactor aged, Fe (and Mn) oxides were removed by reductive dissolution, thereby generating P as a by−product in an analogous manner to

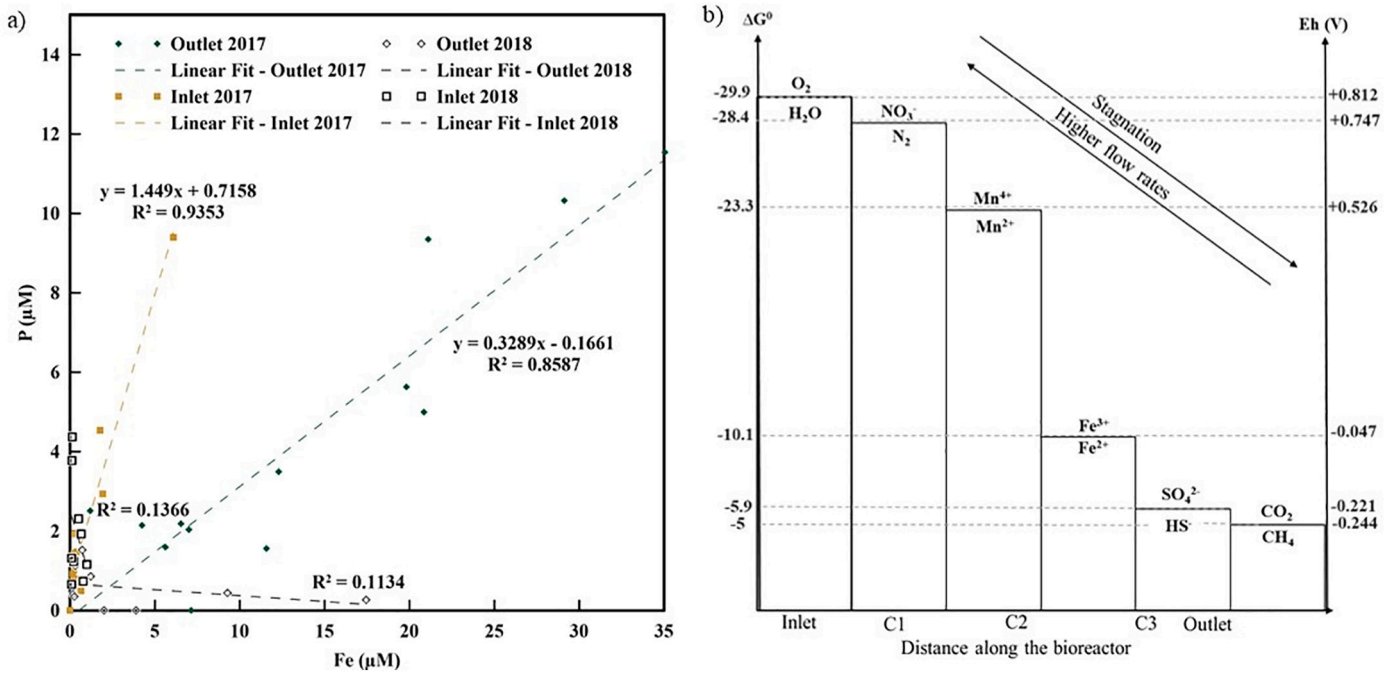


**Fig. 3.** a) Correlations between iron (Fe) and phosphorus (P) at the inlet and outlet of the Tatuanui bioreactor in the 2017 and 2018 drainage seasons. b) The redox ladder shown in the context of the Tatuanui DBR (ΔGo = Gibbs free energy change of reaction relative to the standard hydrogen electrode, Eh = redox potential in volts).

**Table 1**
Comparison of the P removal rates of the woodchip bioreactors.

| Effluent | Bioreactor media | pH | DO (g $m^3$) | N-$NO_3$ removal rate (g $m^3$ $d^{-1}$) | P removal rate (g $m^3$ $d^{-1}$) | Reference |
|---|---|---|---|---|---|---|
| Agricultural drainage | Woodchips | 5.6–7.1 | 0.0–0.2 | 0.7–1.6 | 0.6 | Rivas et al. (2020a, 2020b) |
| Agricultural drainage | Sawdust | | | 0.25 | 0 | Schipper and Vojvodić-Vuković (2000) |
| Glasshouse | Woodchips and sawdust | | 0–15 | 10 | 0 | Schipper et al. (2010) |
| Treated domestic | Woodchips and sawdust | | 0–15 | 11 | 0 | |
| Treated dairy shed | Woodchips and sawdust | | 0–15 | 1.4 | 0 | |
| Agricultural drainage | Woodchips with steel by products | 6.1–6.8 | | 10 | 0.3 | Hua et al. (2016) |
| domestic wastewater | Woodchips and coconut husk | 7 | 0.8–8.8 | 2.8–12 | 0.2 | Tanner et al. (2012) |
| | Woodchips | 6.6–7.2 | | 40 | 0.4 | Povilaitis et al. (2020) |
| Agriculture tile drainage | Woodchips and activated carbon | | | 45 | 0 | |
| | Woodchips and flaxseed cake | | | 41 | 0 | |
| Mine drainage | Woodchips and steel slag | 7.5–8.4 | | 8.0–18 | 8.8–48 | Christianson et al. (2017) |

arsenic releases common to reduced aquifer environments (Borch et al., 2010; Hartland et al., 2015).

Evidence for a range of redox transformations coupled to anaerobic carbon oxidation is provided by the loss of electron acceptors such as $NO_3^-$ and $SO_4^{2-}$, or by the generation of reduction products such as $Mn^{2+}$, $Fe^{2+}$, and $H_2S$ (Fig. 1). Unlike the mobile, soluble oxidants ($NO_3^-$ and $SO_4^{2-}$), Fe and Mn are insoluble under oxidising conditions and therefore would be readily incorporated during reactor construction (i.e., from surrounding soils, or by attachment to wood chips). This explains why the outlet concentration of their reaction products (soluble $Fe^{2+}$ and $Mn^{2+}$ ions) exceeded the inlet concentration, decaying from initial highs following reactor commissioning, to reach consistently low concentrations by the second half of season 2 (Fig. 1).

### 4.3. Constraining P removal rates under varying source dynamics

Taking our analysis one step further, we can use the correlations reported here between Fe and P at the DBR inlet and outlet to evaluate P removal performance (due to biological P assimilation) under varying source dynamics. The steep Fe:P inlet ratio is consistent with the adsorption of P on colloidal iron oxides, which as widely observed elsewhere (Sposito, 2004), have large specific surface areas and correspondingly high P-adsorption capacities. Outlet concentrations of Fe and P also remained correlated throughout season 1, but the Fe:P ratio at the outlet was higher, suggesting preferential loss of P, relative to Fe along the flow path.

While Fe(II) cannot be considered truly conservative (e.g. because of potential formation of Fe(II) precipitates, adsorption and so on), if we assume that $Fe^{2+}$ was minimally removed within the reactor (an assumption supported by negative $FeOH_3$ saturation index values (Fig. 2)), the outlet Fe concentrations can be used to estimate the equivalent autochthonous (i.e. *in-situ*) P supply to the reactor microorganisms (i.e. P that was originally associated with Fe (hydr)oxides incorporated during bioreactor construction, then subsequently released during Fe oxide dissolution). Using Eq. (1) (derivation of this equation is included in the supplementary information), we estimated the rate of biological P uptake within the Tatuanui DBR associated with Fe oxide dissolution (P removal rate $_{(FeOx)}$; Fig. 4) and compared this to the apparent P removal rate (P removal rate $_{(app)}$; Eq. (2)). The rates are then combined (Eq. (3)) to infer the overall P removal rate, accounting for

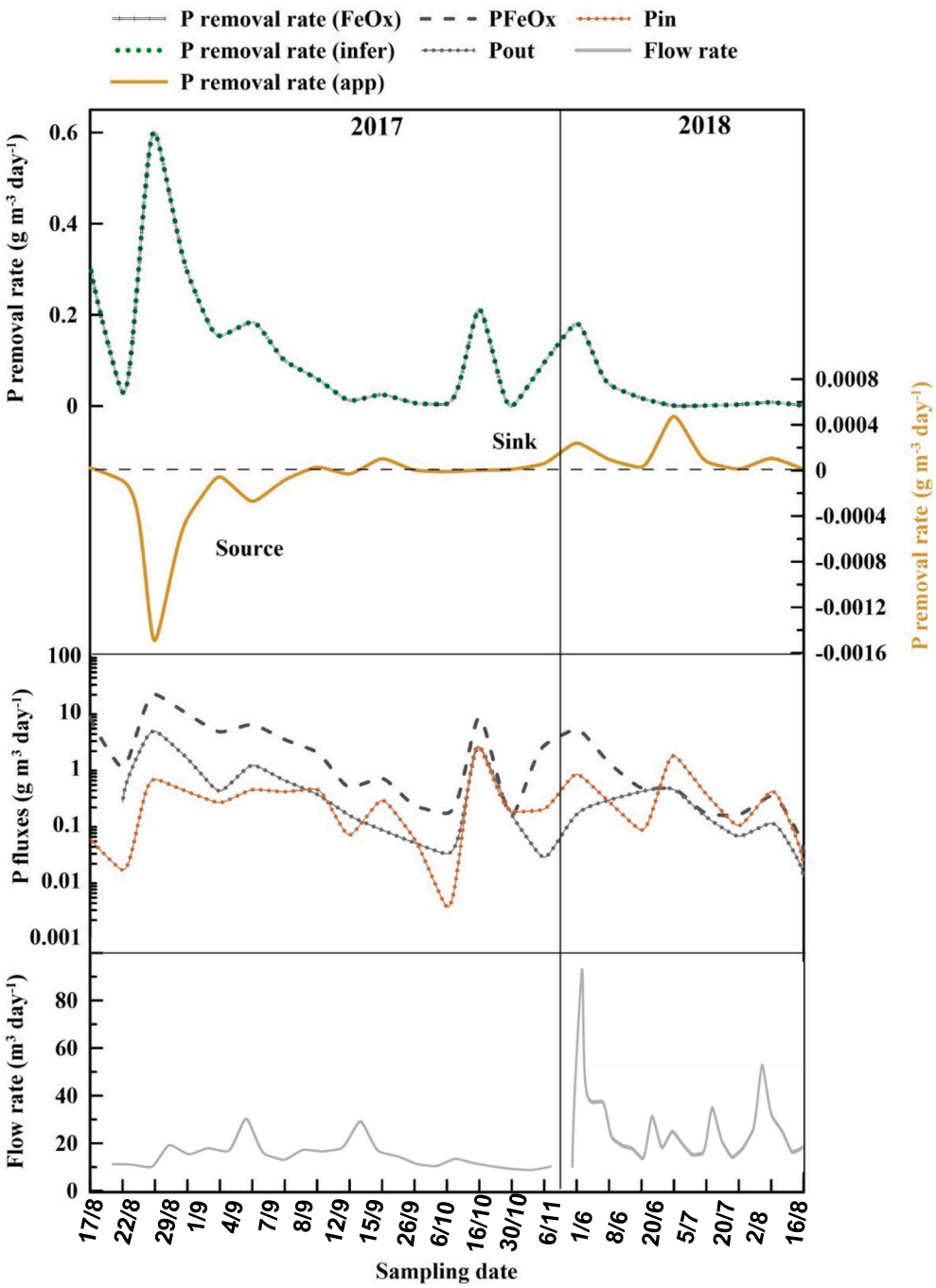


**Fig. 4.** Phosphorus (P) removal in the Tatuanui bioreactor across drainage seasons. Upper panel: apparent (P removal rate $_{(app)}$), iron (hydr)oxide associated (P removal rate $_{(FeOx)}$), and the overall inferred rate (P removal rate $_{(inf)}$). Middle panel: the corresponding observed and calculated P fluxes; lower panel: flow rate through the bioreactor.

allochthonous and autocthonous P sources (P removal rate $_{(inf)}$; Fig. 4). This analysis suggests that biological removal of P was highest following commissioning and was dominated by autocthonous P sources associated with iron (hydr)oxide dissolution. Inferred rates fluctuated throughout season 1, leading to pseudo steady−state removal in season 2, following exhaustion of Fe(III) (hydr)oxides (Fig. 4).

$$\text{P removal rate}_{(FeOx)} = \frac{[(Fe_{out}\ 1.449 + 0.7158) - P_{out}]Q}{V_s \varnothing} \quad (1)$$

$$\text{P removal rate}_{(app)} = \frac{[P_{in} - P_{out}]Q}{V_s \varnothing} \quad (2)$$

$$\text{P removal rate}_{(inf)} = \text{P removal rate}_{(app)} + \text{P removal rate}_{(FeOx)} \quad (3)$$

where Vs is the saturated volume of the bioreactor ($m^3$), $\varnothing$ is the effective or drainable porosity, and Q is the flow rate ($m^3$ $day^{-1}$). The drainable porosity and the saturated volume of the bioreactor were 46.2 % and 56.3 $m^3$, respectively (Rivas et al., 2020a, 2020b; Rivas et al., 2023). The equivalent inlet P concentration is estimated in Eq. (1), by substitution of the linear equation between inlet Fe and P (**Fig. 3**), based on the assumption that Fe entering the reactor inlet was present as insoluble Fe(III) hydro(oxides) and was representative of native soil-derived Fe oxides incorporated during reactor construction. We note that positive $Fe(OH)_3$(a) saturation index values were recovered for all

inlet solutions modelled in PHREEQC (Fig. 2)).

The assumptions made in the above analysis are further supported by PHREEQC modelling, which indicates that no P−bearing mineral phases were oversaturated within the reactor. Furthermore, the saturation index for amorphous $Fe(OH)_3$ remained negative (undersaturated) from the first mid−well (C1) to the outlet, i.e., indicating no formation of Fe (II) or Fe(III) species above the level needed to form insoluble products. Therefore, the dissolution of native iron hydr(oxide) minerals within the reactor (Fig. 2) is unlikely to have been reversed by either oxidation or formation of secondary/tertiary mineral phases between the site of Fe (III) reduction and the outlet. This modelling also indicates that P is likely to have remained as orthophosphate, or as organic P, once incorporated into biomass.

We hypothesise that during the process of dissolution of Fe (hydr) oxides in season 1 and season 2, P was preferentially retained through biological uptake. One implication of this hypothesis is that bioreactors may naturally shift from P−sources to P−sinks across their lifetimes, but with higher rates of P removal at the inception of drainage seasons due to the higher availability of insoluble Fe hydr(oxides), potentially indicating luxury uptake as microbiological communities become established (Khoshmanesh et al., 2002).

Several studies have demonstrated that the biological uptake of P by polyphosphate accumulating organisms, leads to P storage as intracellular polyphosphate polymers under both aerobic and anoxic conditions (Sathasivan, 2009). Specific microorganisms break down and release these polyphosphates under anaerobic conditions (Kerrn-Jespersen and Henze, 1993; Meinhold et al., 1999). However, in general, the rate of P uptake is considerably higher under anaerobic conditions than in aerobic conditions (Wu et al., 2023). Comeau et al. (1987) and Gerber et al. (1987) have suggested that nitrate may serve as an electron acceptor during P uptake reactions under anaerobic conditions, which may enhance P bioaccumulation rates in denitrifying bioreactors.

### 4.4. Potential for augmentation of denitrifying bioreactors with iron oxide surfaces to enhance P removal

As seen in other environments characterised by oscillating redox gradients (Saeed et al., 2018), natural Fe (and Mn) (hydr)oxides incorporated into woodchip bioreactors, become rapidly reduced under N − limiting conditions, leading to the release of P, previously adsorbed to Fe (hydr)oxide surfaces. We can anticipate that any colloidal or particulate iron oxides present in drainage water will also undergo dissolution within DBRs, producing $Fe^{2+}$ ions and $HPO_4^-$ among other secondary reaction products (at pH 5–6). This finding begs the question: can we harness these processes to enhance the removal of P from agricultural drainage water?

One approach is to use iron-based adsorbents for P removal. However, the evolution of redox chemistry in any DBR system will certainly have a major impact on the deployment of functionalized materials intended for P adsorption. Using PHREEQC 3.0 we calculated the saturation indices (SI) and the equilibrium speciation of all major and minor dissolved ions present in the Tatuanui bioreactor to evaluate the most effective positioning of a hypothetical P−sorbing substrate and to make recommendations for bioreactors more generally. Our results suggest that inlet water was commonly oversaturated with respect to amorphous Fe (hydr)oxide ($SI_{Fe(OH)3} > 0$), implying that introduced Fe−oxide−media would remain intact, and potentially grow through Fe precipitation if the media were placed close to the inlet. Conversely, the hypothetical media would be dissolved if positioned deeper within the bioreactor.

From a practitioner's standpoint, the introduction of Fe−based media in DBRs needs to be informed by an understanding of the potential for Fe oxide dissolution through dissimilatory Fe(III) reduction, and potential deterioration in media performance due to the formation and growth of biofilms on the surfaces of the functionalized media. Biofilms are complex systems composed of multicellular communities, organic and inorganic substances that grow on surfaces (Rao et al., 1997). There have been reports of biofilm formation under aphotic conditions that are analogous to conditions within DBRs. The formation of biofilms on any functionalized media (i.e., Fe−oxide−coated woodchips), could potentially inhibit P adsorption via changes in the electrostatic properties of solid surfaces, and possibly via wholesale changes in the functional chemistry of the biofilm−coated particles. While this remains an open question, our findings based on equilibrium speciation modelling indicate that Fe(III)-based materials would effectively capture additional iron from the influent, promoting the further growth and replenishment of introduced Fe (hydr)oxide surfaces, assuming Fe−media were placed at the inlet of the bioreactor.

To further illustrate this point, we simulated the effect of introducing iron oxides at different positions within the Tatuanui DBR based on the average composition of water at each position (Table 2). In Table 2, positive ΔFeT values indicate a net gain in the solid phase, and negative values indicate a net loss from the solid phase (i.e. dissolution). Based on the Tatuanui monitoring results, a net increase in $Fe(OH)_3$ is possible based on the inlet water reaching equilibrium with Fe oxides (placed at the inlet). For example, the net cumulative effect of Fe precipitation on introduced Fe−functionalized media (in proximity to the inlet of the studied system) could result in a gain of up to 10.9 g of mass and 1.39 $cm^3$ of volume based on a cumulative flow of 1000 $m^3$, assuming complete conversion of Fe to $Fe(OH)_3$ (s).

This exercise shows that iron-based composites would not be expected to withstand anaerobic conditions within the bioreactor, but would likely be retained if positioned in proximity to the reactor inlet due to higher dissolved oxygen levels (Tatuanui 2021 drainage season dataset).

## 5. Conclusions

We show that following denitrifying bioreactor commissioning, an initial period of phosphorus emission can occur. This initial period of P emission likely results from 1) the release of labile P from fresh wood chips (which declines rapidly as they age), and 2) the reductive dissolution of soil−derived iron (hydr)oxides. These autochthonous P sources resulted in net P emission throughout the initial phase of operation at the Tatuanui bioreactor. However, once both processes were exhausted, the denitrifying bioreactor became and remained, a net P sink. Furthermore, our analysis of Fe−P variations in the bioreactor supports the interpretation that P uptake rates scale with supply, with higher initial uptake of P in the reactor inferred during the phase of Fe (hydr) oxide dissolution. This analysis is extended to consider the potential for incorporating Fe−oxide based media within denitrifying bioreactors. We conclude that if positioned close to the reactor inlet, Fe−oxides should be preserved by the oxic conditions, and indeed may even grow, in effect potentially replenishing their P adsorption capacity over time.

## CRediT authorship contribution statement

**Gimhani N. Perera:** Writing – original draft, Visualization, Validation, Software, Methodology, Investigation, Formal analysis, Data curation. **Dorisel Torres Rojas:** Writing – review & editing, Project

**Table 2**
Net predicted deviation in iron mass for iron−based composites within different bioreactor compartments (Tatuanui 2021 drainage season dataset).

| Sampling wells | ΔFeT (μM) |
|---|---|
| Inlet | 0.03 |
| C1 | −41.7 |
| C2 | −20.0 |
| C3 | −26.7 |
| Outlet | −54.1 |

administration, Methodology, Investigation, Formal analysis, Conceptualization. **Aldrin Rivas:** Writing – review & editing, Supervision, Data curation. **Greg Barkle:** Writing – review & editing, Supervision. **Brian Moorhead:** Supervision, Resources, Methodology. **Louis A. Schipper:** Funding acquisition. **Rupert Craggs:** Supervision, Funding acquisition. **Adam Hartland:** Writing – review & editing, Visualization, Software, Project administration, Funding acquisition, Formal analysis, Conceptualization.

## Declaration of competing interest

The authors declare no competing interests.

## Data availability

Data and code provided in the supplementary information.

## Acknowledgements

Primary funding for this research was provided by the Ministry for Business Innovation and Employment (MBIE) under Contract No. C01X1818, through the program "Te Waiora Joint Institute for Freshwater Management," a collaboration between the University of Waikato and NIWA. We would like to thank James Owers (Lincoln Agritech Ltd.) for assistance with bioreactor maintenance, Reza Moghaddam (University of Waikato) for fieldwork support, Annie Barker (University of Waikato) for help with laboratory analysis and Amir Mohammadi (University of Waikato) for guidance with fieldwork. This research was made possible by the Mourits family for allowing us to conduct our study on their farmland.

## Appendix A. Supplementary data

Supplementary data to this article can be found online at https://doi.org/10.1016/j.scitotenv.2024.170478.

## References

Addy, K., Gold, A.J., Christianson, L.E., David, M.B., Schipper, L.A., Ratigan, N.A., 2016. Denitrifying bioreactors for nitrate removal: a meta-analysis. J. Environ. Qual. 45 (3), 873–881.

Blowes, D.W., Robertson, W.D., Ptacek, C.J., Merkley, C., 1994. Removal of agricultural nitrate from tile-drainage effluent water using in-line bioreactors. J. Contam. Hydrol. 15 (3), 207–221. https://doi.org/10.1016/0169-7722(94)90025-6.

Borch, T., Kretzschmar, R., Kappler, A., Cappellen, P.V., Ginder-Vogel, M., Voegelin, A., Campbell, K., 2010. Biogeochemical redox processes and their impact on contaminant dynamics. Environ. Sci. Technol. 44 (1), 15–23. https://doi.org/10.1021/es9026248.

Charlton, S.R., Parkhurst, D.L., 2011. Modules based on the geochemical model PHREEQC for use in scripting and programming languages. Comput. Geosci. 37 (10), 1653–1663. https://doi.org/10.1016/j.cageo.2011.02.005.

Christianson, L., Bhandari, A., Helmers, M., Kult, K., Sutphin, T., Wolf, R., 2012. Performance evaluation of four field-scale agricultural drainage denitrification bioreactors in Iowa. Transactions of the ASABE 55 (6), 2163–2174. https://dr.lib.iastate.edu/handle/20.500.12876/1059.

Christianson, L.E., Lepine, C., Sibrell, P.L., Penn, C., Summerfelt, S.T., 2017. Denitrifying woodchip bioreactor and phosphorus filter pairing to minimize pollution swapping. Water Res. 121, 129–139. https://doi.org/10.1016/j.watres.2017.05.026.

Christianson, L.E., Cooke, R.A., Hay, C.H., Helmers, M.J., Feyereisen, G.W., Ranaivoson, A.Z., McMaine, J.T., McDaniel, R., Rosen, T.R., Pluer, W.T., Schipper, L. A., Dougherty, H., Robinson, R.J., Layden, I.A., Irvine-Brown, S.M., Manca, F., Dhaese, K., Nelissen, V., von Ahnen, M., 2021. Effectiveness of denitrifying bioreactors on water pollutant reduction from agricultural areas. Trans. ASABE 64 (2), 641–658. https://doi.org/10.13031/trans.14011.

Comeau, Y., Oldham, W.K., Hall, K.J., 1987. Dynamics of carbon reserves in biological dephosphatation of wastewater. In: Ramadori, R. (Ed.), Biological Phosphate Removal From Wastewaters. Pergamon, pp. 39–55. https://doi.org/10.1016/B978-0-08-035592-4.50010-9.

Corbett, T.D.W., Dougherty, H., Maxwell, B., Hartland, A., Henderson, W., Rys, G.J., Schipper, L.A., 2020. Utility of 'diffusive gradients in thin-films' for the measurement of nitrate removal performance of denitrifying bioreactors. Sci. Total Environ. 718, 135267 https://doi.org/10.1016/j.scitotenv.2019.135267.

Damasceno, B.S., da Silva, A.F.V., Ferreira, M.C., de Melo, A.N., Leite, D.M.G., de Araújo, A.C.V., 2023. A facile and eco-friendly hydrothermal synthesis of magnetic graphite nanocomposite and its application in water purification. Colloids Surf. A Physicochem. Eng. Asp. 670, 131528 https://doi.org/10.1016/j.colsurfa.2023.131528.

David, M.B., Gentry, L.E., Cooke, R.A., Herbstritt, S.M., 2016. Temperature and substrate control woodchip bioreactor performance in reducing tile nitrate loads in east-central Illinois. J. Environ. Qual. 45 (3), 822–829. https://doi.org/10.2134/jeq2015.06.0296.

Dougherty, H. (2018). Hydraulic Evaluation of a Denitrifying Bioreactor With Baffles Urbana, IL: University of Illinois.] Master thesis.

Dougherty, H., Cooke, R.A.C., Bhattarai, R., Christianson, L., 2020. Design flow and nitrate removal evaluation of a wide denitrifying bioreactor with baffles. Ecol. Eng. 158, 106068 https://doi.org/10.1016/j.ecoleng.2020.106068.

Dzombak, D.A., Morel, F.M.M., 1991. Surface Complexation Modeling: Hydrous Ferric Oxide. Wiley. https://books.google.co.nz/books?id=LGBtoHNUbWwC.

Fan, Y., Essington, M., Jagadamma, S., Zhuang, J., Schwartz, J., Lee, J., 2022. The global significance of abiotic factors affecting nitrate removal in woodchip bioreactors. Sci. Total Environ. 848, 157739 https://doi.org/10.1016/j.scitotenv.2022.157739.

Gerber, A., De Villiers, R., Mostert, E., Van Riet, C., 1987. The phenomenon of simultaneous phosphate uptake and release, and its importance in biological nutrient removal. In: Biological Phosphate Removal from Wastewaters. Elsevier, pp. 123–134. https://doi.org/10.1016/B978-0-08-035592-4.50016-X.

Hartland, A., Larsen, J.R., Andersen, M.S., Baalousha, M., O'Carroll, D., 2015. Association of arsenic and phosphorus with iron nanoparticles between streams and aquifers: implications for arsenic mobility. Environ. Sci. Technol. 49 (24), 14101–14109. https://doi.org/10.1021/acs.est.5b03506.

Hua, G., Salo, M.W., Schmit, C.G., Hay, C.H., 2016. Nitrate and phosphate removal from agricultural subsurface drainage using laboratory woodchip bioreactors and recycled steel byproduct filters. Water Res. 102, 180–189. https://doi.org/10.1016/j.watres.2016.06.022.

Kerrn-Jespersen, J.P., Henze, M., 1993. Biological phosphorus uptake under anoxic and aerobic conditions. Water Res. 27 (4), 617–624. https://doi.org/10.1016/0043-1354(93)90171-D.

Khoshmanesh, A., Hart, B.T., Duncan, A., Beckett, R., 2002. Luxury uptake of phosphorus by sediment bacteria. Water Res. 36 (3), 774–778. https://doi.org/10.1016/S0043-1354(01)00272-X.

Lepine, C., Christianson, L., Davidson, J., Summerfelt, S., 2018. Woodchip bioreactors as treatment for recirculating aquaculture systems' wastewater: a cost assessment of nitrogen removal. Aquac. Eng. 83, 85–92. https://doi.org/10.1016/j.aquaeng.2018.09.001.

Meinhold, J., Arnold, E., Isaacs, S., 1999. Effect of nitrite on anoxic phosphate uptake in biological phosphorus removal activated sludge. Water Res. 33 (8), 1871–1883. https://doi.org/10.1016/S0043-1354(98)00411-4.

Mohammadi, A., Corbett, T., French, A., Lehto, N.J., Hadfield, J., Jarman, P., Sandwell, D., Shokri, A., Schipper, L., Hartland, A., 2022. Application of diffusive gradients in thin films for monitoring groundwater quality. ACS ES&T Water 2 (4), 518–526. https://doi.org/10.1021/acsestwater.1c00279.

Oehmen, A., Carvalho, G., Freitas, F., Reis, M.A., 2010. Assessing the abundance and activity of denitrifying polyphosphate accumulating organisms through molecular and chemical techniques. Water Sci. Technol. 61 (8), 2061–2068. https://doi.org/10.2166/wst.2010.976.

Parkhurst, D. L. (1995). *User's guide to PHREEQC, a computer program for speciation, reaction-path, advective-transport, and inverse geochemical calculations* [Report] (95–4227). (Water-Resources Investigations Report, Issue. U. S. G. Survey. http://pubs.er.usgs.gov/publication/ wri954227.

Povilaitis, A., Matikienė, J., Vismontienė, R., 2020. Effects of three types of amendments in woodchip-denitrifying bioreactors for tile drainage water treatment. Ecol. Eng. 158, 106054 https://doi.org/10.1016/j.ecoleng.2020.106054.

Rao, T.S., Rani, P.G., Venugopalan, V.P., Nair, K.V.K., 1997. Biofilm formation in a freshwater environment under photic and aphotic conditions. Biofouling 11 (4), 265–282. https://doi.org/10.1080/08927019709378336.

Reese, B.K., Finneran, D.W., Mills, H.J., Zhu, M.-X., Morse, J.W., 2011. Examination and refinement of the determination of aqueous hydrogen sulfide by the methylene blue method. Aquat. Geochem. 17, 567–582.

Rivas, A., Barkle, G., Stenger, R., Moorhead, B., Clague, J., 2020a. Nitrate removal and secondary effects of a woodchip bioreactor for the treatment of subsurface drainage with dynamic flows under pastoral agriculture. Ecol. Eng. 148, 105786 https://doi.org/10.1016/j.ecoleng.2020.105786.

Rivas, A., Singh, R., Horne, D.J., Roygard, J., Matthews, A., Hedley, M.J., 2020b. Contrasting subsurface denitrification characteristics under temperate pasture lands and its implications for nutrient management in agricultural catchments. J. Environ. Manag. 272, 111067 https://doi.org/10.1016/j.jenvman.2020.111067.

Rivas, A., Barkle, G., Sarris, T., Park, J., Kenny, A., Maxwell, B., Stenger, R., Moorhead, B., Schipper, L., Clague, J., 2023. Improving accuracy of quantifying nitrate removal performance and enhancing understanding of processes in woodchip bioreactors using high-frequency data. Sci. Total Environ. 880, 163289 https://doi.org/10.1016/j.scitotenv.2023.163289.

Saeed, H., Hartland, A., Lehto, N.J., Baalousha, M., Sikder, M., Sandwell, D., Mucalo, M., Hamilton, D.P., 2018. Regulation of phosphorus bioavailability by iron nanoparticles in a monomictic lake. Sci. Rep. 8 (1), 17736. https://doi.org/10.1038/s41598-018-36103-x.

Sanchez Bustamante-Bailon, A.P., Margenot, A., Cooke, R.A.C., Christianson, L.E., 2022. Phosphorus removal in denitrifying woodchip bioreactors varies by wood type and water chemistry. Environ. Sci. Pollut. Res. Int. 29 (5), 6733–6743. https://doi.org/10.1007/s11356-021-15835-w.

Sathasivan, A. (2009). Biological phosphorus removal processes for wastewater treatment. *Water and wastewater treatment technologies. Oxford (UK): encyclopedia of life support systems (EOLSS)*, 1-23.

Schipper, L.A., Vojvodić-Vuković, M., 2000. Nitrate removal from groundwater and denitrification rates in a porous treatment wall amended with sawdust. Ecol. Eng. 14 (3), 269–278.

Schipper, L.A., Robertson, W.D., Gold, A.J., Jaynes, D.B., Cameron, S.C., 2010. Denitrifying bioreactors—an approach for reducing nitrate loads to receiving waters. Ecol. Eng. 36 (11), 1532–1543. https://doi.org/10.1016/j.ecoleng.2010.04.008.

Shahid, M.K., Kim, Y., Choi, Y.-G., 2019. Magnetite synthesis using iron oxide waste and its application for phosphate adsorption with column and batch reactors. Chem. Eng. Res. Des. 148, 169–179. https://doi.org/10.1016/j.cherd.2019.06.001.

Sharrer, K.L., Christianson, L.E., Lepine, C., Summerfelt, S.T., 2016. Modeling and mitigation of denitrification 'woodchip' bioreactor phosphorus releases during treatment of aquaculture wastewater. Ecol. Eng. 93, 135–143. https://doi.org/10.1016/j.ecoleng.2016.05.019.

Sposito, G., 2004. The Surface Chemistry of Natural Particles. Oxford University Press.

Stumm, W., Morgan, J.J., 1996. Aquatic Chemistry: Chemical Equilibria and Rates in Natural Waters. Wiley. https://books.google.co.nz/books?id=xvZOAAAAMAAJ.

Sun, Y., Peng, Y., Zhang, J., Li, X., Zhang, Q., Zhang, L., 2020. Effect of endogenous metabolisms on survival and activities of denitrifying phosphorus removal sludge under various starvation conditions. Bioresour. Technol. 315, 123839 https://doi.org/10.1016/j.biortech.2020.123839.

Tanner, C.C., Sukias, J.P.S., Headley, T.R., Yates, C.R., Stott, R., 2012. Constructed wetlands and denitrifying bioreactors for on-site and decentralised wastewater treatment: comparison of five alternative configurations. Ecol. Eng. 42, 112–123. https://doi.org/10.1016/j.ecoleng.2012.01.022.

Thapa, U., Ahiablame, L., Kjaersgaard, J., Hay, C., 2023. Field evaluation of four denitrifying woodchip bioreactors for nitrogen removal in eastern South Dakota, United States. Sci. Total Environ. 855, 158740 https://doi.org/10.1016/j.scitotenv.2022.158740.

Viollier, E., Inglett, P.W., Hunter, K., Roychoudhury, A.N., Van Cappellen, P., 2000. The ferrozine method revisited: Fe(II)/Fe(III) determination in natural waters. Appl. Geochem. 15 (6), 785–790. https://doi.org/10.1016/S0883-2927(99)00097-9.

Wu, T., Yang, S.-S., Zhong, L., Pang, J.-W., Zhang, L., Xia, X.-F., Yang, F., Xie, G.-J., Liu, B.-F., Ren, N.-Q., Ding, J., 2023. Simultaneous nitrification, denitrification and phosphorus removal: what have we done so far and how do we need to do in the future? Sci. Total Environ. 856, 158977 https://doi.org/10.1016/j.scitotenv.2022.158977.

Zaman, M., Kim, M., Nakhla, G., 2021. Simultaneous nitrification-denitrifying phosphorus removal (SNDPR) at low DO for treating carbon-limited municipal wastewater. Sci. Total Environ. 760, 143387 https://doi.org/10.1016/j.scitotenv.2020.143387.